The International Journal of Advanced Manufacturing Technology (2024) 133:1733–1747
https://doi.org/10.1007/s00170-024-13852-w

ORIGINAL ARTICLE

# Research on the influence of die head arrangement on the precision of discontinuous deformation in multi-points stretch-bending of profiles

Yu Wen[1] · Ce Liang[1] · Yi Li[1] · Jicai Liang[1]

Received: 28 September 2023 / Accepted: 26 May 2024 / Published online: 3 June 2024


**Abstract**
This paper proposes and develops a novel flexible 3D multi-point stretch-bending and twisting (3D MPSBT) forming equipment with six degrees of freedom to manufacture profiles with different bending radii and twisting angles at a lower tooling cost. Due to the discretization of the machine, the deformation characteristics and forming accuracy of the profiles differ from those of continuous molds. The size of the forming error for rectangular profiles is investigated by employing two different arrangements and numbers of dies. The results show that the forming errors occur in the free deformation zone due to stress effects. When the number of dies is the same, arranging the dies uniformly along the formed arc length yields higher accuracy in the shape of the formed profile. For a rectangular hollow aluminum profile with half the length of 1500 mm, the forming error in the free deformation zone of the profile can be reduced to less than 0.6 mm by using 12 die units arranged along the arc length. However, when the dies are uniformly arranged along the pre-deformation length of the profile, the minimum forming error exceeds 0.6 mm when the number of dies increases to 15. The minimum number of dies required for forming different bending radii is determined. Finally, the accuracy of the numerical simulation and the feasibility of forming complex-shaped aluminum profiles using the 3D MPSBT machine is validated through experiments.

**Keywords** Multi-point bending · Die arrangement · Profile · Forming accuracy

## 1 Introduction

Aluminum profiles are widely used in products from industries such as ships, aerospace, rail vehicles, and automobiles due to their lightweight, which can reduce fuel consumption and $CO_2$ emissions [1, 2]. In addition, aluminum profiles can be made into various complex cross-sectional shapes according to different needs. Profiles with specific curved shapes have high strength and rigidity, facilitating the connection between different parts and saving space, reducing product production costs. With the increasing demands for quality and quantity in various fields, it is essential to mass-produce aluminum workpieces with more complex target shapes and higher precision at low cost [3].

✉ Ce Liang
liangce@jlu.edu.cn

[1] Key Laboratory of Automobile Materials, College of Materials Science and Engineering, Ministry of Education, Jilin University, Changchun, Jilin 130025, China

Traditional profile bending methods include drawing bending, rotary drawing bending, roller bending, and coiling bending, but these traditional forming methods are limited to two-dimensional planar bending deformation [4]. Researchers have recently started to study various three-dimensional bending-forming methods for profiles. Six main pieces of equipment are used for the three-dimensional bending of metal profiles. Table 1 shows the six forming principles or devices and their characteristics. Welo and Granly [5] proposed the concept of free bending and developed a free-bending machine that drives the profile or tube to complete deformation through guide rails and bending die, with the advantages of fast bending speed and no need for re-clamping. This machine can produce tubing for automotive components with almost any bending radius. However, this method is sensitive to material properties and quickly leads to geometric shape inaccuracy in the final part. Chatti et al. [6, 7] designed a flexible three-dimensional profile bending forming equipment and studied the spatial torque superimposed bending process (TSS). Superimposing torque effectively reduces

**Table 1** Main profile 3D bending facilities

| Forming method | Schematic diagram | Key features | Ref. |
|---|---|---|---|
| Free bending | 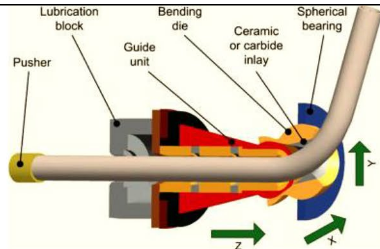 | • Developed for tube cross-section and profile<br>• Fast bending speed<br>• Suitable for manufacturing medium-sized components | [5] |
| Spatial torque superimposed bending process (TSS) | 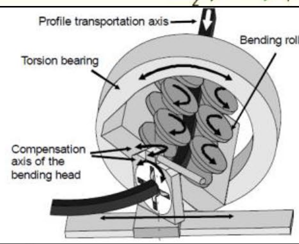 | • Applicable to profiles of any cross-sectional shape and length<br>• No need for a propulsion system | [6] |
| Spatial tubes bending and twisting | 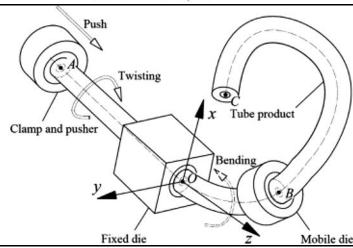 | • Suitable for spatial bending deformation of circular section pipes<br>• Forming speed has a significant impact on the target shape | [8] |
| Flexible 3D stretch bending | 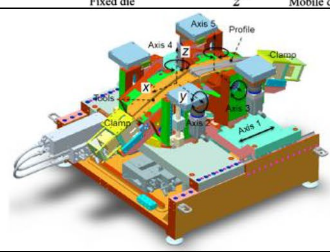 | • Suitable for 3D bending of profiles with different cross-sections<br>• For significantly different bending radii and lengths of profiles, mold replacement is required. | [9] |
| Flexible 3D multi-point stretching and bending machine | 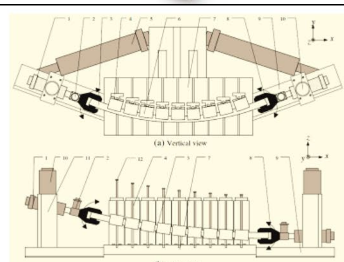 | • Suitable for profiles with various cross-sectional shapes<br>• The processable length range is 1.5 m to 10 m.<br>• When the cross-sectional shape varies, the mold head body needs to be replaced. | [15] |
| Roller-type 3D multi-point bending machine | 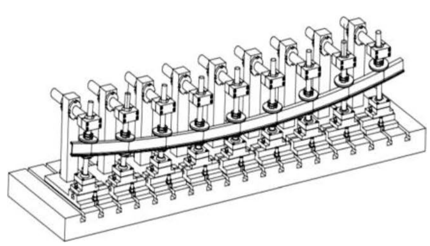 | • Suitable for profiles with various cross-sectional shapes<br>• The processable length range is 1.5 m to 10 m.<br>• No need to replace the roller head when the cross-sectional shape varies. | [16] |

springback during profile bending, avoids damage to the profile, and adds compensating torque to avoid unnecessary twisting of the profile. This equipment can process profiles of any length and interface, but there is still significant springback when the profile length is considerable. Wu et al. [8] realized the combined deformation of space bending and twisting of circular tubes using a fixed die, a movable die, and a clamp and theoretically predicted the springback of the tube. Welo et al. [9, 10] developed a new three-dimensional profile drawing machine with the die divided into two halves and using multi-axis control to increase the die's flexibility and thus increase profile size diversity. However, due to the limitation of die groove shape and size, the range of producible target shapes still needs to be improved. Using discrete dies to form complex plates and profiles has recently become a hot research direction [11–14]. Liang et al. [15] developed a flexible multi-point profile stretch-bending machine that discretizes the conventional continuous die into multiple unit dies. The target shape die surface is constructed by moving and rotating the unit dies with the die body. For different target shape profiles, only the position and angle of the unit dies need to be changed. The processable profile length is 1.5 to 10 m. Later, Liang et al. [16] simplified the die unit bodies above to roller units and developed the second-generation multi-point drawing machine, which omitted to rotate the die body during profile bending, improving production efficiency. Products made from these two flexible, three-dimensional multi-point stretch-bending machines are widely used as high-speed rail vehicle frames. The above profile processing methods have effectively realized the three-dimensional bending of profiles. However, with the continuous enhancement of requirements for energy saving, emission reduction, and lightweight, more complex drawing parts are needed to achieve this goal further. Complex target products with higher aerodynamic performance can be manufactured through combined bending and twisting deformation of profiles, especially non-circular cross-sectional profiles.

This study developed the third-generation stretch-bending machine based on the previous two generations of Liang's machines, changing the structure of the multi-point die units and the motion mode of the die body to realize the combined deformation of bending and twisting of profiles, meeting the demand for complex shaped profile components in today's society. The working principle and motion trajectory calculation method of the machine are introduced. The influence of die head arrangement on part shape accuracy when bending rectangular cross-section profiles with 3D MPSBT is studied by numerical simulation, and the accuracy of numerical simulation results is verified through experiments.

## 2 Working principle and analytical model of 3D MPSBT

### 2.1 Working principle of 3D MPSBT

In order to achieve the 3D stretch-bending and twisting forming process of profiles, a 3D MPSBT machine is designed and manufactured based on its working principle. Figure 1a shows the machine's schematic CAD model, consisting of a base plate, a pair of clamping devices, and die head control devices. Each die head control device provides five degrees of freedom, specifically:

- A rectangular key at the bottom of the control device controls the translational motion along axis 1 in the y-z plane.
- The forming module is controlled by the sliding block moving up and down on the vertical threaded axis, which controls the translational motion in the x direction (axis 2).
- The swinging head controlled by the vertical threaded axis rotating around axis 2 controls the rotational motion in the y-z plane.
- The forming module embedded in the mold control device controls the rotational motion in the x-y plane around axis 4.
- The rotational motion in the x-z plane is controlled by the positioning disc on the sliding block around axis 3.

Hydraulic servo actuators control the motion of the clamps. Each forming module's displacement and rotation angles are calculated to drive the profiles to undergo three-dimensional bending and twisting deformation. Figure 1c and d depict the aluminum profile-forming process. Before forming, the control device's position is adjusted to the mold surface position after the profile is bent in the y-z plane. The clamping device drives the profile to bend, embedding it into the die head. Then, under the driving force of the clamping device, the profile bends in the x-z plane, and the process stops when all the die heads reach the set positions and angles. Subsequently, the twisting process begins and ends when all the forming modules rotate to the limit plate-controlled limit positions.

By changing the spatial position, position, and orientation angles of the die heads in space, the flexibility of the 3D stretch-bending and twisting machine can be enhanced to accommodate profiles with different contours. Changing the number of control devices can accommodate profiles of different lengths. For profiles with different cross-sections, only the embedded components, i.e., the die heads on the module control device, need to be replaced. Therefore, the equipment features reconfigurable mold surfaces, enabling the bending process of profiles with thousands of

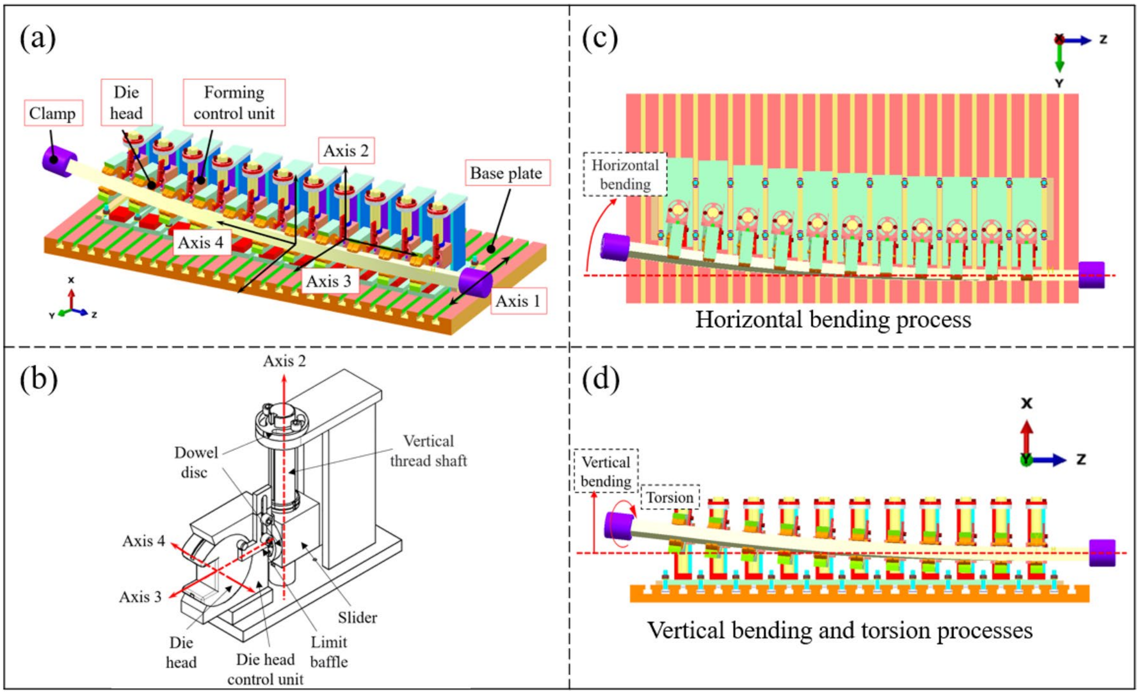


**Fig. 1** **a** 3D MPSBT machine; **b** multi-point forming control unit; **c** horizontal bending process; **d** vertical bending and twisting process

target shapes. When the forming effect is not satisfactory, adjusting the position and twisting angle of the die head unit overcomes the difficulties of traditional fixed mold surfaces in mold repair. The profile bending and twisting forming process can be performed quickly and efficiently, reducing the number of mold repairs and saving costs in mold development and manufacturing. However, since the die heads are discrete units, controlling the deformation of the profiles in the non-contact area with the die heads becomes challenging, leading to a decrease in forming accuracy. Therefore, research is needed to explore process measures for improving the forming quality of the fabricated components.

## 2.2 Analytical model of bending moment-curvature relationship of profiles

In order to obtain an accurate product shape, the relationship between part stress and forming curvature needs to be determined. An analytical model of the bending moment-curvature relationship is needed. The strain at any point on the profile is:

$$\epsilon = \kappa y \tag{1}$$

where $\kappa$ is the curvature of the neutral layer, $y$ is the distance of any point on the cross-section of the profile to the neutral layer plan, and $\varepsilon$ is the total strain of the material. In the profile forming process, it is assumed that the elastic and plastic components can express the total strain, and the plastic component is far greater than the elastic component during forming. Assuming the profile material obeys the simple LUDWICK constitutive law [5], and the cross-section of the profile is a rectangle with height $H$ and width $B$, then the plastic bending moment on the cross-section is:

$$M^* = \int_{-\frac{H}{2}}^{\frac{H}{2}} \sigma y dA = \int_{-\frac{H}{2}}^{\frac{H}{2}} \sigma\,(\epsilon) yB\, dy = \int_{-\frac{H}{2}}^{\frac{H}{2}} K(\kappa y)^n yBdy \tag{2}$$

where $K$ is the strength coefficient, and $n$ is the strain-hardening exponent. Since a hollow rectangular cross-section profile is used, the internal cavity moment $m^*$ should be subtracted when calculating the bending moment. The applied bending moment $M$ is:

$$M = M^* - m^* \tag{3}$$

where $m^*$ is the moment of the internal cavity with depth $h$ and width $b$. After deformation, the profile will springback. The curvature change "$\widehat{\kappa}$" can be defined as:

$$\widehat{\kappa} = \frac{M}{EI} \tag{4}$$

where $E$ is the elastic modulus, and $I$ is the moment of inertia of the profile cross-section.

The radius $R'$ of the profile after springback can be expressed as:

$$R' = \frac{1}{\kappa} - \frac{M}{EI} \quad (5)$$

When the clamps drive the bending of the profile, the profile will undergo elastic and plastic deformation. Under the drive of the clamps, the profile gradually contacts the die head units. In addition, due to a contact zone and free deformation zone during bending, the actual contact point between the profile and die differs from the theoretical contact point obtained by geometric calculation. It means that the bending angle of the free deformation zone of the profile will be different from the applied bending angle.

Figure 2 shows the profile part deformation structure between adjacent two die heads when a multi-point die forms the part, where $v_{AB}$ is the offset of point $B$ relative to point $A$, $L$ is the actual length of the endpoint connection line of the free deformation zone of the profile, $\theta$ is the angle between the perpendicular line of the edge of arc ADB and the connection line of adjacent two die head units, $L_0$ is the straight line distance from $A$ to the theoretical contact point of the profile cross-section, and $R$ is the theoretical bending radius.

In Fig. 2, point $B$ is the contact point between the edge of the contact area of the die head unit and the profile, and point $A$ is the reference point of the die head. The angle $\alpha_{BA}$ between the segment BA and the connecting line of the reference points of adjacent two die heads is:

$$\alpha_{BA} = \int_L \kappa(x)dx \quad (6)$$

where $\kappa(x)$ is the bending curvature of the profile. Compared with the applied bending angle, the angle corresponding to $v_{AB}$ is minimal. Thus, $\alpha_{BA}$ and $\theta$ are very close angles. As can be seen from Fig. 2, the calculation formula for $\alpha_{BA}$ from a geometric point of view is:

$$\alpha_{BA} = \theta - \frac{v_{AB}}{L} = \frac{L - \frac{L_0}{2}}{R} - \frac{(L_0 - L)^2}{2RL} \quad (7)$$

Introducing a dimensionless quantity $\xi = L_0/L$, the above equation can be simplified to:

$$\theta = \frac{L_0}{2R}(\xi - \frac{1}{\xi} + 1) \quad (8)$$

All the parameters are constants. When $L$ gets closer to $L_0$, the obtained $\theta$ is closer to $\alpha_{BA}$. However, it requires a narrower die head. A narrower die head has a smaller contact area with the profile, which makes it difficult to control the curvature of the free deformation zone of the profile. When the distance between adjacent dies is significant, the curvature of the profile's free deformation zone will be smaller than the theoretical value. Increasing the number of dies can improve the forming accuracy of the profile, but this will cause difficulties in die installation and increase manufacturing costs. Therefore, it is necessary to study the die arrangement method and the minimum number of die heads that can produce qualified parts.

## 3 Finite element model of 3D Profile bending process

### 3.1 Assembly finite element model

This paper uses ABAQUS software to perform computational analysis of the multi-point stretch bending process.

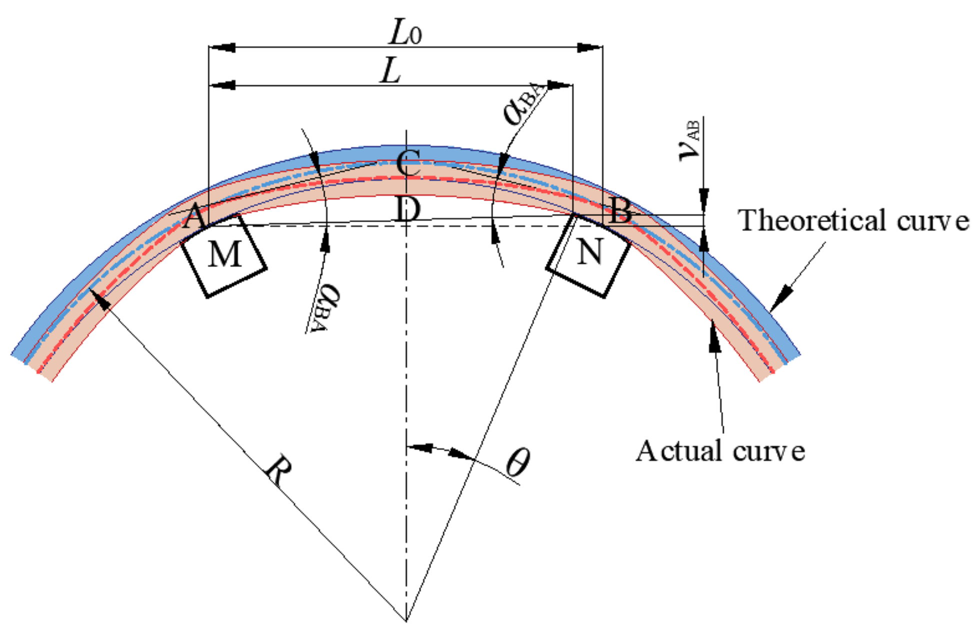


**Fig. 2** Structure before unloading

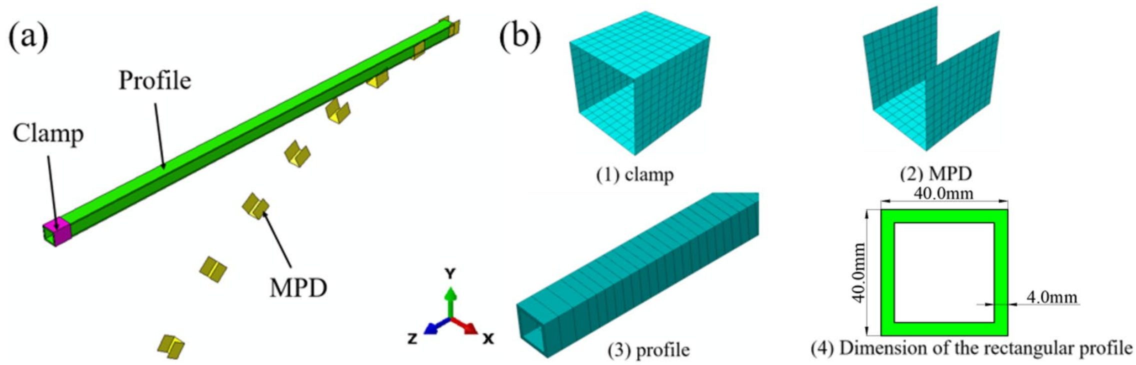


**Fig. 3** Finite element model of multi-point stretch-bending and twisting forming: **a** assembly diagram of 3D MPSBT; **b** mesh division and dimensions of the profile

In ABAQUS software, die head units, clamps, and profile parts are established, assembled, and meshed; analysis steps are defined; loads are defined; and other preparatory work for simulation calculation is performed. Since profile deformation is an extensive deformation process, considering the convergence problems caused by geometry, material, and contact nonlinearity, the bending process uses dynamic, implicit analyses.

This paper studies a rectangular cross-section profile. Figure 3a shows the assembly finite element model of an 8 die heads bending a 3100 mm long profile. Due to the symmetry of profile deformation, half of it is used for numerical calculation. The boundary condition of the symmetry plane is defined as ZSYMM. The model comprises a rectangular profile, clamps, and 8 die-head units. The dies are equally spaced in the axis-z direction, the clamps are bound and constrained to the profile, and the inner surface of the die and the outer surface of the rectangular profile are defined as surface-to-surface contact, standard friction is hard contact, and tangential friction coefficient is 0.1.

The profile is a three-dimensional deformable body with a mesh type of C3D8R. The clamp and die heads are simplified to three-dimensional shells and set as rigid bodies with mesh type of R3D4 rigid unit since they do not deform. The scaling factor for mass is 300. The mesh division and profile cross-sectional dimensions are shown in Fig. 3b.

## 3.2 Material properties

This paper studies a 6005A aluminum alloy profile. The uniaxial stress-strain tensile test is carried out on the profile. The nominal stress and strain obtained from the experiment must be converted into true stress and true plastic strain for numerical simulation calculation, with the conversion formula as Eq. (9). Table 2 shows the material parameters of 6005A aluminum alloy. The true stress-strain curve is shown in Fig. 4. The mechanical properties of the aluminum profile obey the Mises yield criterion, and the elastoplastic constitutive behavior is isotropic.

$$\begin{cases} \sigma_{real} = \sigma_{norm}(1 + \epsilon_{norm}) \\ \epsilon^{p} = \ln\left(1 + \epsilon_{norm}\right) - \frac{\sigma_{norm}(1+\epsilon_{norm})}{E} \end{cases} \quad (9)$$

**Table 2** Material performance parameters of 6005A aluminum profile

| Brand | Density ($\rho$) | Young's modulus ($E$) | Yield strength ($\sigma_s$) | Poisson's ratio ($\nu$) |
|---|---|---|---|---|
| 6005A | 2.71 g/cm³ | 71,320 MPa | 264.33 MPa | 0.33 |

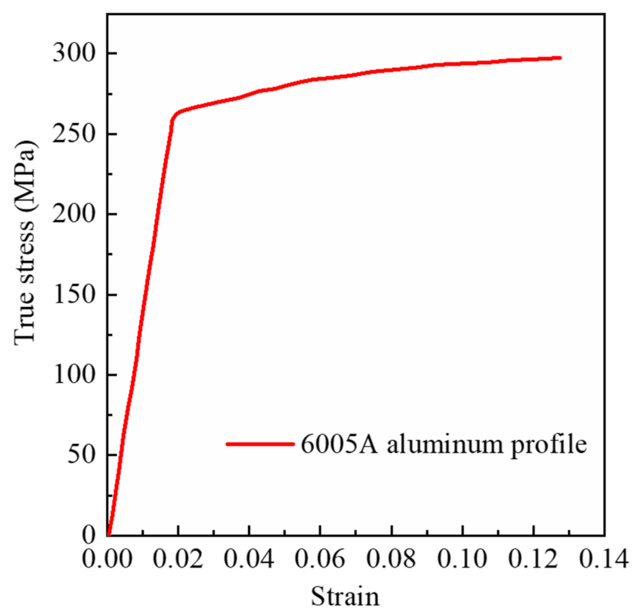


**Fig. 4** Stress-strain curve of 6005A aluminum profile

where $\sigma_{real}$, $\sigma_{norm}$, $\varepsilon^{p}$, and $\varepsilon_{norm}$ represent the true stress, nominal stress, true plastic strain, and nominal strain, respectively. $E$ is the Young's modulus.

### 3.3 Design of die head and clamp motion trajectories

The curvatures of the profile in the horizontal and vertical directions can be continuously variable or fixed. In order to study the influence of process parameters on forming accuracy in the free deformation zone of profiles, the target curvature of profiles is designed as fixed curvature. The clamps drive the profile to complete the deformation process. Figure 5 is the profile-forming trajectory. To precisely control the shape of the workpiece, we use displacement control to control the movement of the profile. First, the profile is stretched axially by $\delta_{pr}$ to reach the plastic state. Then, the profile undergoes horizontal bending deformation in the y-z plane, and each die head's initial placement angle and position are calculated by Eqs. (10) and (11).

$$\alpha_i = \arcsin\left(\frac{z_i}{R_h - b}\right), \quad (i = 1,2,3,\cdots,n) \tag{10}$$

$$y_i = \left(R_h - b\right) \times \left(1 - cos\alpha_i\right), \quad (i = 1,2,3,\cdots n) \tag{11}$$

where $z_i$ is the distance from the $i$th die head unit to the center of the profile, $R_h$ is the horizontal bending radius of the bottom surface of the profile, $b$ is the distance from the reference point of the die head unit to the bottom surface of the profile, $\alpha_i$ is the horizontal rotation angle of the $i$th die, $y_i$ is the distance the $i$th die moves along the axis-y.

The clamp trajectory is:

$$\begin{cases} Y = \left(R_h + d_1\right)(1 - \cos\ \theta) + \left[\frac{L_0}{2} + \delta_{pr} - \theta(R_h + d_1)\right] \sin\ \theta \\ Z = \frac{L_0}{2} + \delta_{pr} - \left(R_h + d_1\right) \sin\ \theta - \left[\frac{L_0}{2} + \delta_{pr} - \theta(R_h + d_1)\right] \cos\ \theta \end{cases} \tag{12}$$

where $Y$ and $Z$ represent the translation distances of the clamp in the y direction and z direction, respectively, $d_1$ is the distance from the reference point of the clamp to the bottom surface of the profile, $\theta$ is the horizontal angle between the die head close to the clamp and the symmetry plane of the profile, $L_0$ is the original length of the entire profile, $\delta_{pr}$ is the pre-stretch amount for each clamp. Finally, post-stretching of the profile is required. The post-stretching of the clamps can be calculated as:

$$\begin{cases} \delta_x = 0 \\ \delta_y = \delta_{po}\sin\theta \\ \delta_z = \delta_{po}\cos\theta \end{cases} \tag{13}$$

where $\delta_{po}$ is the post-stretching amount of the clamps along the axial direction of the profile and $\delta_x$, $\delta_y$, and $\delta_z$ are the components of $\delta_{po}$ in the $x$, $y$, and $z$ directions, respectively.

## 4 Results and analysis

### 4.1 Influence of discrete dies on stress-strain distribution of the profile

Using 8 die head units, a half-length of the profile is analyzed for bending. The pre-stretching and post-stretching amounts are 1% of the length of the unclamped region of the profile, with a bending radius of 1500 mm. Figure 6 illustrates the axial lines on the upper and lower surfaces of the profile. Figure 7 shows the stress and strain diagrams of the axial lines $m$ and $n$ on the upper and lower surfaces of the profile at the end of the deformation. On the upper surface, the stress is higher in the contact area compared to the non-contact area due to the more significant bending deformation. On the lower surface, the stress is lower in the contact area and higher in the free deformation area because the free deformation area experiences tremendous tensile

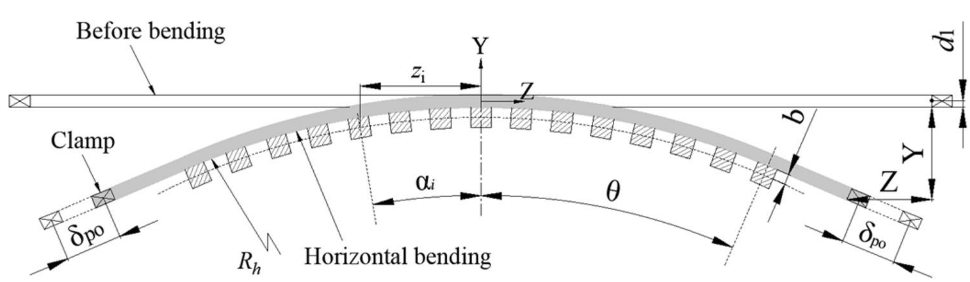


**Fig. 5** Profile bending process

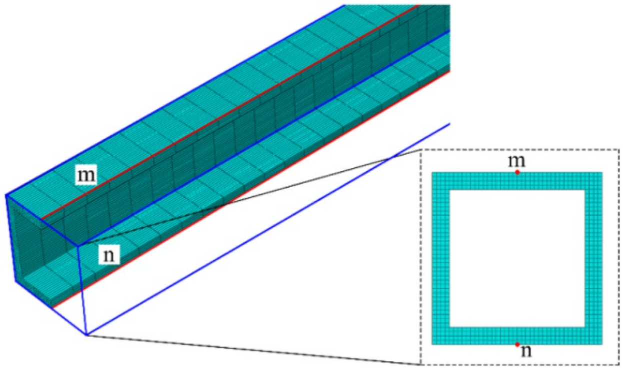


**Fig. 6** Axial lines *m* and *n* on the upper and lower surfaces of the profile

stress during the post-stretching stage, while the contact area experiences compressive stress. Figure 8 displays the stress distribution of each profile near the contact area with the mold after selecting the cross-section according to Fig. 6. The stress distribution trend is similar for each contact area.

In Fig. 8b, axial tensile and compressive stress influence is more significant, with a linear distribution from bottom to top. Therefore, the surface stress on the symmetry plane is higher than at other positions. Figure 8c to h shows the contact areas from the second to the seventh die head unit. It can be observed from the figures that as the distance from the symmetry plane increases, the side panel and upper and lower surface stresses in the contact area become larger, resulting in the strain distribution shown

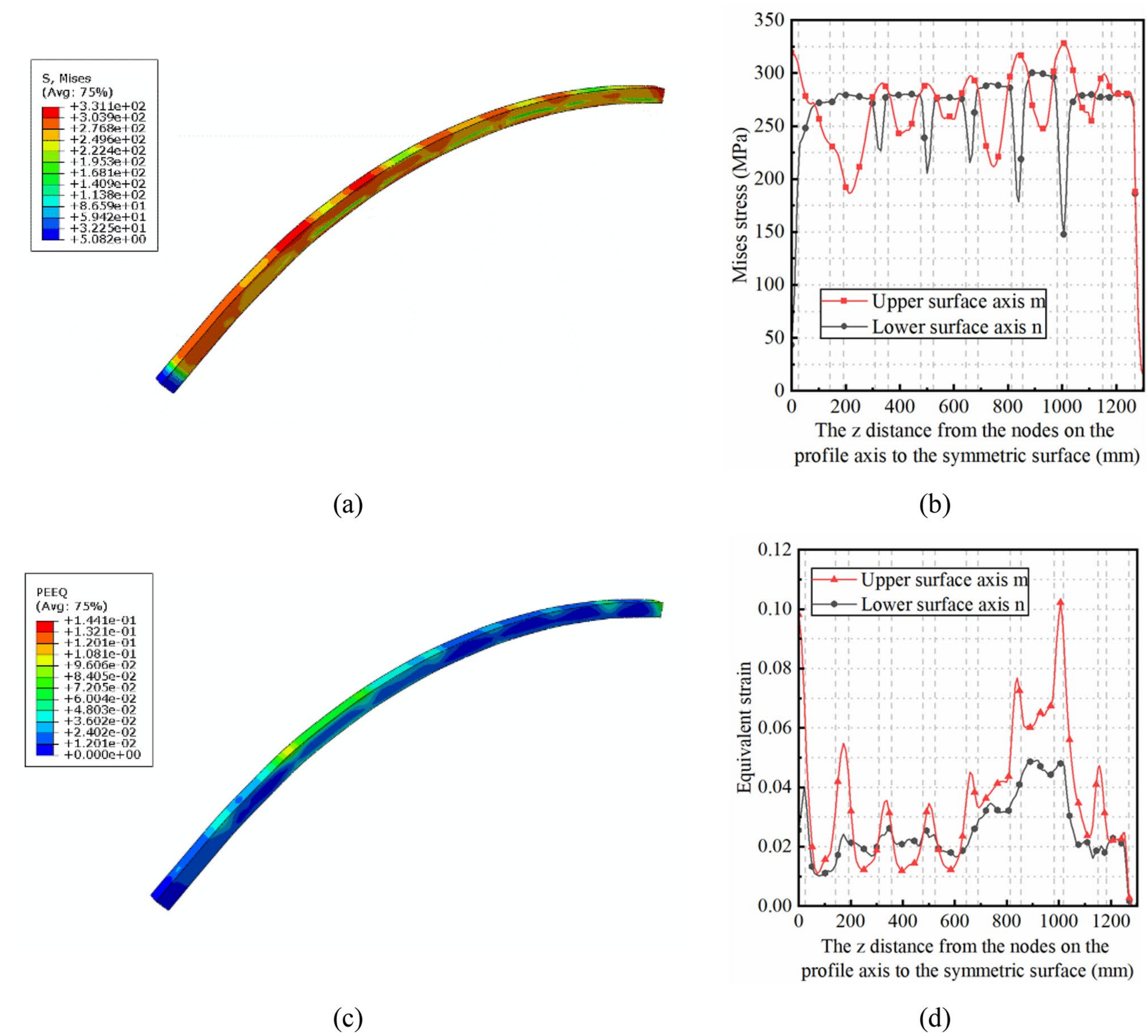


**Fig. 7** Stress distribution and equivalent strain distribution of axial lines *m* and *n* of the profile after the deformation

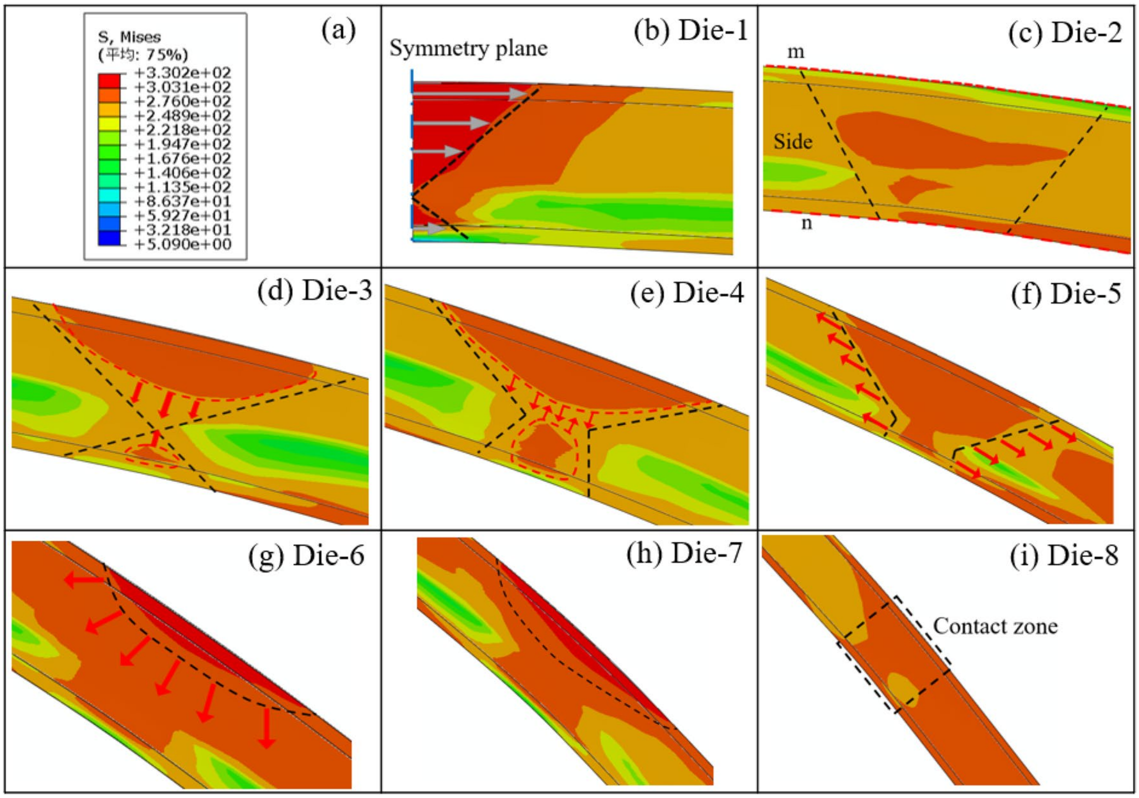


**Fig. 8** Variation of stress in different contact areas

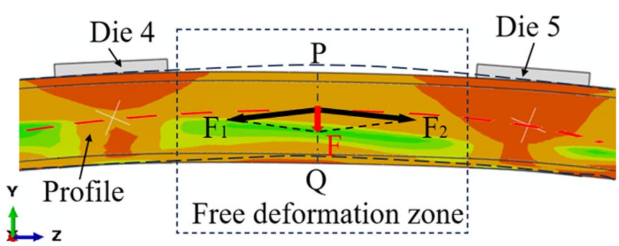


**Fig. 9** Analysis of the influence of stress on deformation in the non-contact area

in Fig. 7c and d. Due to the combined effects of friction and bending, slight stress concentration and larger strains occur at these positions. Figure 8i represents the contact area closer to the clamp at the eighth die head unit. In this position, the tensile stress is predominant, resulting in decreased stress concentration and a more uniform and extensive tension.

Figure 9 shows the stress distribution in the non-contact area between the fourth and fifth mold units, which is analyzed to understand the causes of forming errors. In the free deformation zone, the cross-section experiences a downward force along the y-axis, resulting in a collapse and forming error. Ultimately, the forces acting on the profile's section PQ must reach equilibrium. Similarly, there will be downward concavity in the non-contact areas between other adjacent mold units. It is especially pronounced in the free deformation zone between the seventh and eighth die head units, with larger tensile forces. Consequently, the downward force along the y-axis is more remarkable, leading to a more noticeable collapse.

## 4.2 Influence of discrete die layout on axial forming accuracy

Figure 10a shows the difference between the actual position coordinates of nodes on the profile axial line *m* and line *n* and the target position coordinates after forming. In the contact zone, the forming error on the lower surface is less than 0.02 mm. In the non-contact zone, the maximum forming error on the lower surface is about 1 mm. Only the forming error between the outermost two die heads is significantly larger, reaching a maximum of 2.74 mm. The main reasons for this phenomenon are as follows: Firstly, since the dies are arranged at equal intervals in the z-direction, the distance between the outermost two die units is farther, resulting in a longer free deformation zone of the profile and more complex control of deformation. Secondly, there is lateral friction between the contact zones of the profile and die head

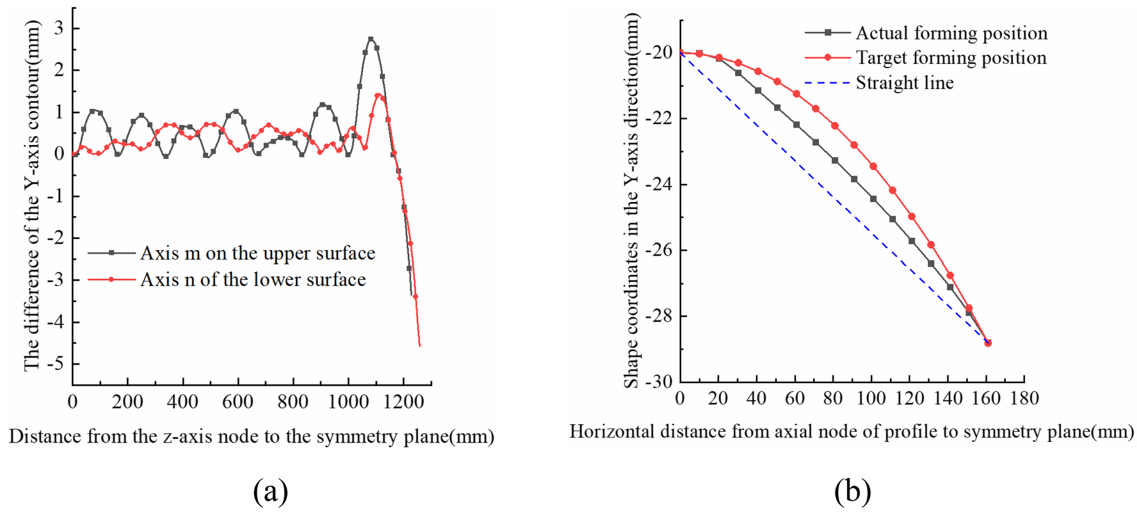


**Fig. 10** The difference between the actual formed contour and the target contour at each point on the axis *m* and *n*: **a** difference between node coordinates and target values; **b** forming position characteristics of each node on axial line *n* between adjacent die heads of the profile

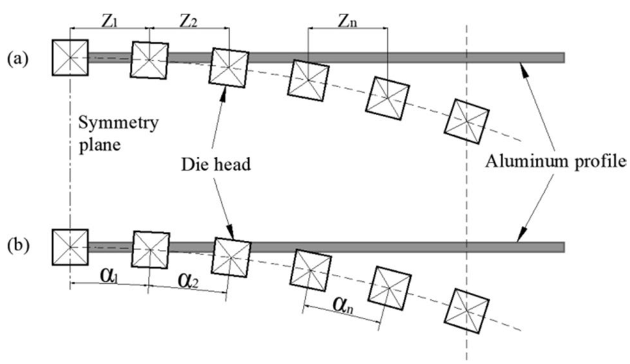


**Fig. 11** Die heads arrangements: **a** equal spacing along the z direction; **b** equal angle arrangement

units. In the post-stretching stage, the profile region between the outermost two dies is subjected to smaller frictional and larger tensile forces, so it is more prone to tensile deformation under the tensile force.

In contrast, the regions far from the clamps experience larger frictional and smaller tensile forces, making it more challenging to undergo tensile deformation and achieve higher forming accuracy. Since the upper surface of the profile is not in direct contact with the die heads and thinning exists, each node has apparent errors, and the overall node error on the upper surface is smaller than that on the lower surface. However, in the contact region, the error between the actual forming position and the theoretical position of nodes on the profile's upper surface is larger than the error in the non-contact zone due to the larger degree of bending. It is opposite to the characteristics of the lower surface. The node with the maximum error on the upper surface is also near the clamp. Figure 10b shows the actual forming position-target forming position of the profile in the y direction between two adjacent die head units on the center plane of symmetry of the profile. Due to the effect of the bending moment, the actual forming shape of the free deformation zone is not entirely linear, which is the same as the analyzed form in Fig. 2.

Theoretically, the more closely discrete die heads are arranged, the larger the contact area between the die heads and parts, and the higher the forming accuracy of parts. However, the associated problem is the difficulty of die arrangement. Therefore, multi-point forming aims to achieve economic forming accuracy using fewer die-head control units for profile forming. Parts are considered qualified when the forming error is less than 0.6 mm. The forming accuracy of the free deformation zone of the profile is related to the number and arrangement of dies and the bending radius. Two different die arrangement methods are shown in Fig. 11. Figure 11(a) shows equal spacing along the z-axis, and Fig. 11(b) shows equal spacing along the arc length after profile deformation. The forming error of the free deformation zone of the profile is studied for 8–15 dies using the two arrangement methods.

The forming error between any two adjacent die heads is not always consistent, as shown in Fig. 12. Due to the larger stretch and bending forces at the profile center symmetry plane and clamp end, the maximum forming error between adjacent die heads first decreases and then increases, reaching a maximum near the clamp.

Figure 13 shows the maximum forming error, i.e., the error between the two dies closest to the clamp, for the two forming methods. It can be seen that with the increase in the number of dies, the maximum forming errors on the upper and lower surfaces of the profile decrease for both arrangements. The maximum error for equal angle arrangement

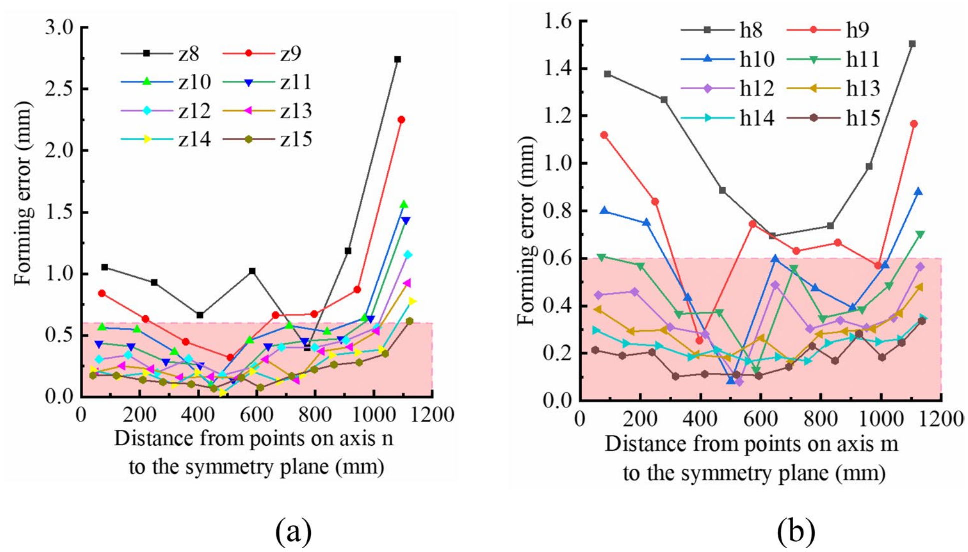


**Fig. 12** Maximum forming error between adjacent die heads of the profile under different die arrangements: **a** equal spacing along z direction; **b** equal angle arrangement

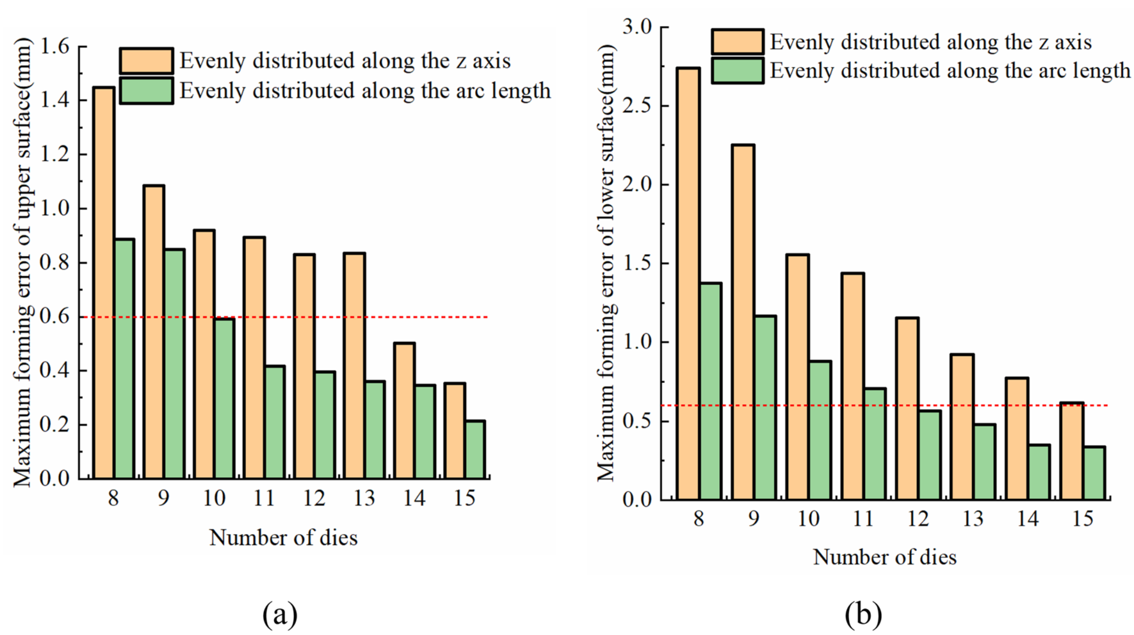


**Fig. 13** Maximum forming error of the profile under different numbers of die heads: **a** maximum error on upper surface; **b** maximum error on lower surface

is significantly smaller with the same number of dies. It is because uniform distribution along the formed arc length avoids the situation of too small distance between die heads near the middle of the profile and too large distance between die heads near the clamp, reducing the length of the free deformation zone at the profile end, making this part closer to the target shape. When using 13 die heads arranged along the axis of the profile, the maximum error on the upper surface is 0.36 mm, and the maximum error on the lower surface is 0.48 mm, meeting the product quality requirements. When using 14 or 15 die heads, the length variation of the free deformation zone is very small. Therefore, when uniformly distributed along the arc length, the error variation on the lower surface is very small, 0.35 mm and 0.34 mm, respectively. By comparing Fig. 13a and b, it can be seen that the upper surface error is about 50% of the lower surface error. Therefore, the forming accuracy of the lower surface needs to be mainly considered in actual forming.

As shown in Figs. 12 and 13, taking the maximum forming error as 0.6 mm, 12 dies arranged with equal angles

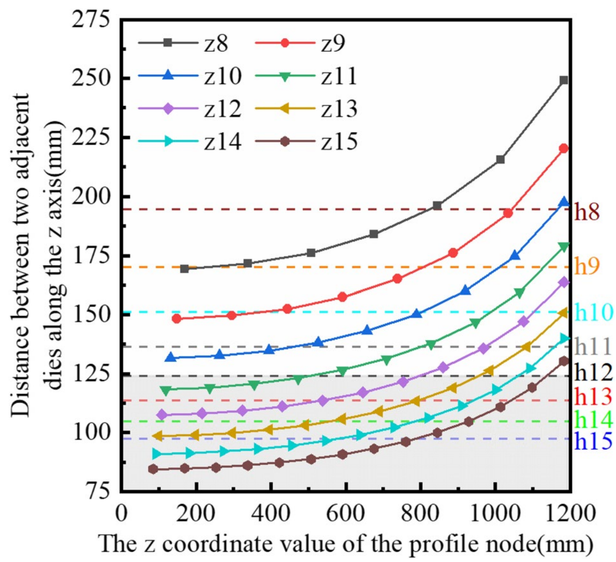


**Fig. 14** Variation of adjacent die spacing along the axial direction of the profile

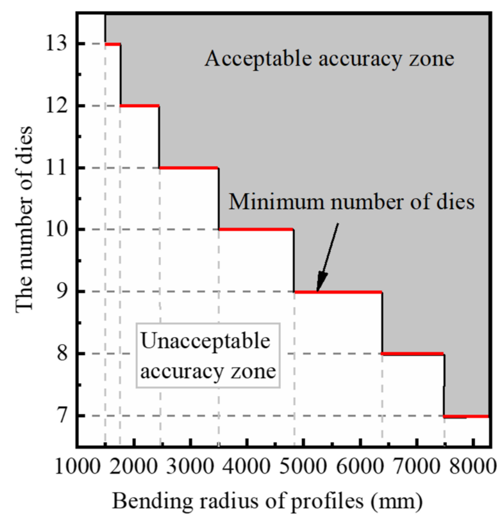


**Fig. 16** Minimum number of die heads required for profile deformation under different bending radii

can meet the requirements under the premise of a bending radius of 1500 mm. Figure 14 shows the z-direction distance between adjacent die heads under different die arrangements and numbers of dies. As shown in Fig. 14, when arranged with 12 equal angles, the z-direction distance between adjacent die heads is 123.93 mm, while the distance between the outermost two die heads is still greater than this value when arranged with 15 equal-spaced die heads. Therefore, as shown in Fig. 13b, the maximum forming error of the profile formed by arranging 15 die heads in the z direction is still more significant than that generated by arranging 12 die heads with equal angles.

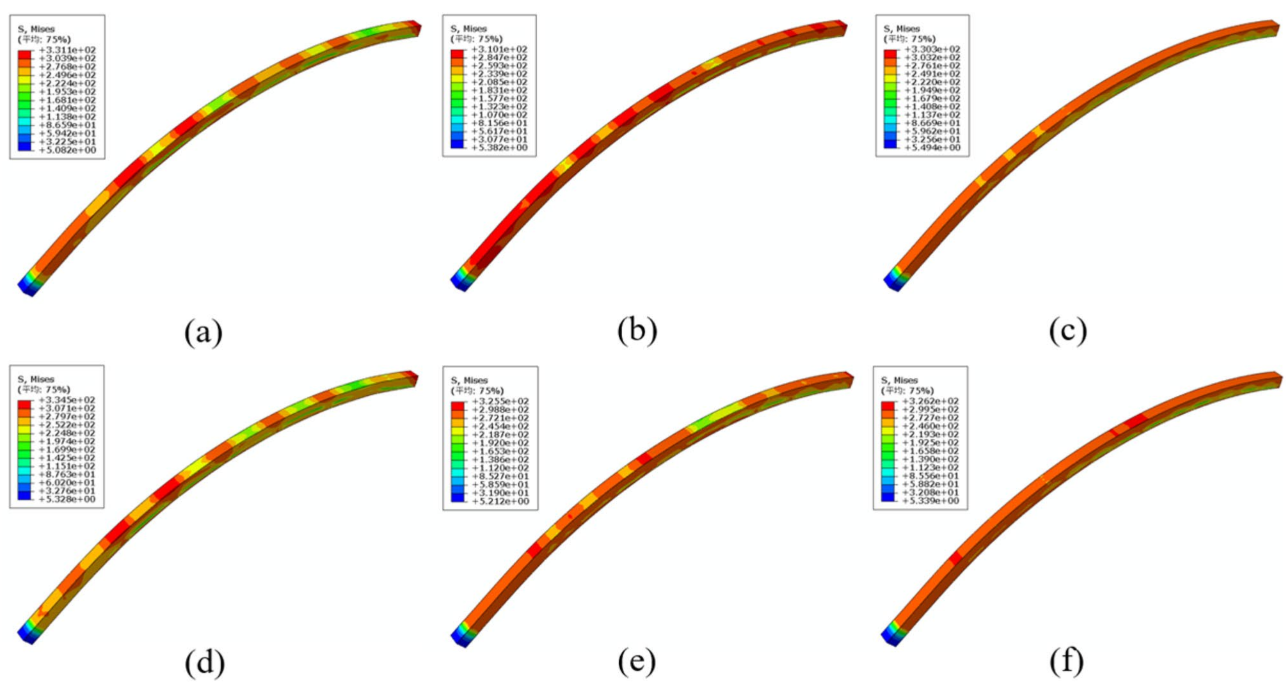


**Fig. 15** Stress distribution with different numbers of die heads and different arrangement modes: **a** 8 die heads are arranged along the z-axis; **b** 11 die heads are arranged along the z-axis; **c** 15 die heads arranged along the z-axis; **d** 8 die heads arranged along the arc length; **e** 11 die heads arranged along the arc length; **f** 15 die heads are arranged along the arc length

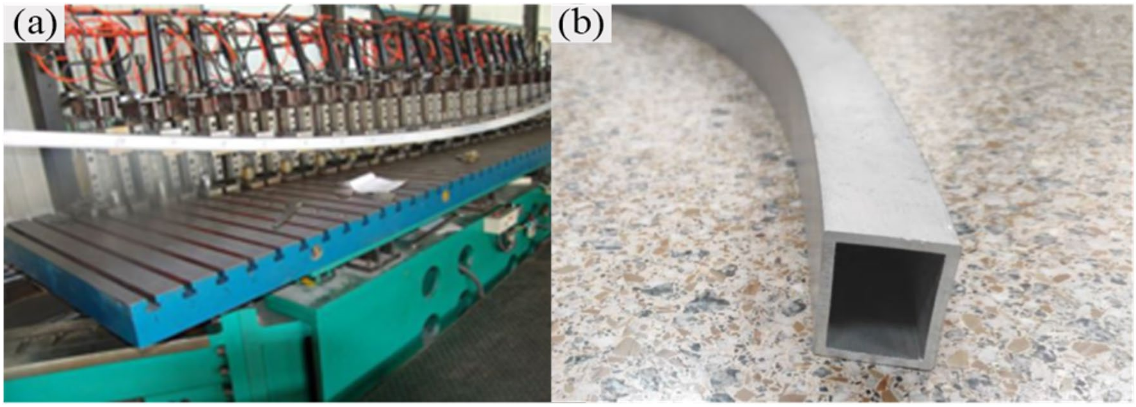


**Fig. 17** **a** 3D MPSBT forming equipment; **b** profile product

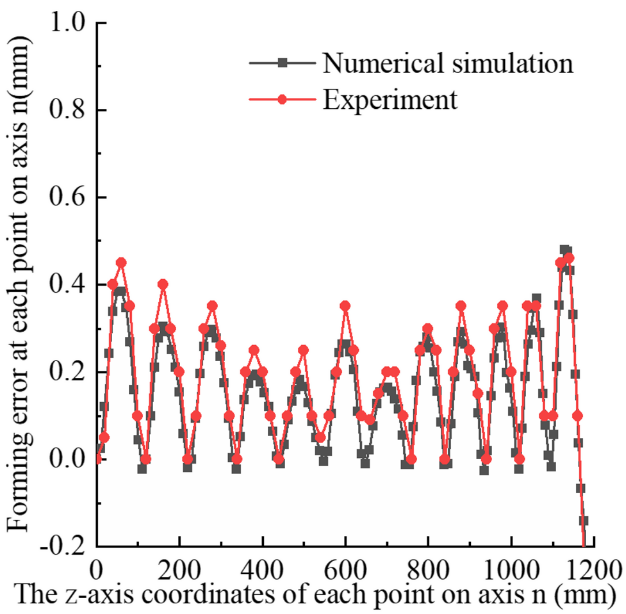


**Fig. 18** Forming error at each point on axial line *n* of lower surface ($R = 1500$ mm)

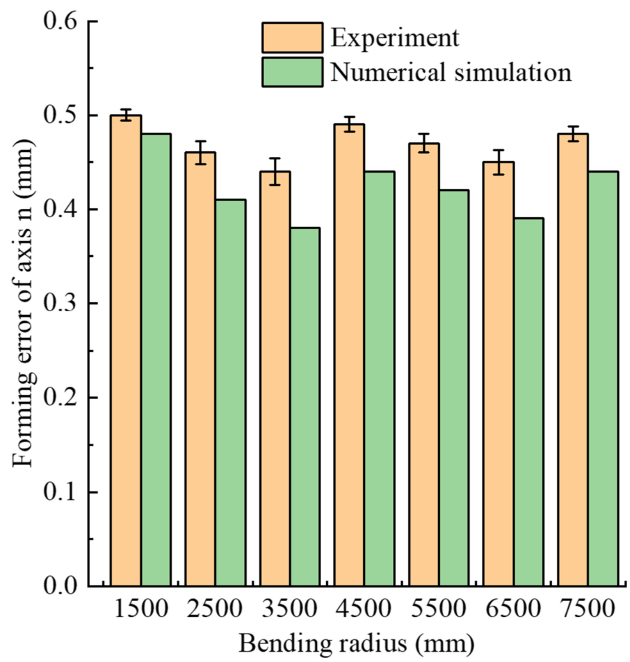


**Fig. 19** Maximum forming error under different bending radii

Figure 15 shows the stress distribution of the profile formed by arranging dies according to schemes (a) and (b) in Fig. 11 with 8, 11, and 15 die heads. As the number of die heads increases, the contact area between the die heads and profile increases, the free deformation zone decreases, and the stress is more difficult to release, so the stress distribution becomes more uniform and larger. Comparing Fig. 15a with d, b with e, and c with f, the stress of the profile arranged uniformly along the arc length is smaller and more uniform for the same number of die heads under different arrangements.

The smaller the bending radius of the profile, the larger the deformation of the profile between two adjacent die heads. Therefore, the smaller the bending radius, the more die heads are required for profile bending, and it is easier to meet the accuracy requirements. When the bending radius is large, the deformation of the profile between the two adjacent die heads is small, and a small number of die heads are needed to meet the accuracy requirements. Figure 16 shows the minimum number of die heads required for profiles to achieve the required accuracy at different bending radii. From 1500 to 8000 mm, several radii are selected for simulation. Each numerical model adopts the arrangement of equal arc length between two adjacent die heads. The dichotomous method is used to find the critical radius at which the number of die heads begins to change. As shown in Fig. 16, when the radius is increased from 1500 to 8000 mm, the number of die heads is reduced from 13 to 7, and the number of die heads is reduced by nearly half. When the radius is 1500 mm, the arc length of the profile between the two adjacent die heads is 113.6 mm. When the radius is 8000 mm, the arc length of the profile between the two adjacent die heads is 195.0 mm.

## 5 Experimental verification

The multi-point stretching bending forming verification device and products are shown in Fig. 17. To study the product's shape accuracy, an NDI large space measurement instrument PRO CMM 3500 optical tracking instrument is used to scan the three-dimensional deformed parts.

Figure 18 compares a rectangular cross-section profile's bending experimental and numerical simulation results with a bending radius of 1500 mm. Measurement points are taken every 20 mm on the axial line of the lower surface of the bending product after the experiment, and the actual forming errors are measured and compared with the simulation results. The trend of the shape error in the experiment is consistent with the shape error in the simulation results, and the maximum forming error occurs between the two die heads closest to the clamp. Due to the influence of external factors in the experiment, the shape error of the experimental product is larger than that of the simulation. However, it is always within the allowable tolerance range.

Twenty-one rectangular profiles are selected for multi-point bending experiments according to the minimum number of die heads required for different bending radii obtained from Fig. 16, with bending radii of 1500 mm, 2500 mm, 3500 mm, 4500 mm, 5500 mm, 6500 mm, and 7500 mm. Three profiles are bent for each radius, the maximum forming error is measured on each profile, and the average value is calculated and compared with the numerical simulation forming error. After comparison, the numerical simulation results are consistent with the experimental results, as shown in Fig. 19. The experimental results verify the accuracy of the numerical simulation results and verify that high-quality three-dimensional stretching bending parts can be produced using this machine.

## 6 Conclusions

In order to meet the production needs of profiles with complex shapes, a three-dimensional multi-point controlled stretching bending forming die with rotatable forming modules around its axis is proposed. Its working principle is introduced, and methods for calculating motion trajectories of forming modules and clamps are proposed. The influence of die head arrangement methods on profile forming quality and improvement methods are discussed through experiments and finite element simulation. The following conclusions can be drawn:

1. The three-dimensional multi-point stretching bending forming equipment with rotatable forming heads around their axes can form shape-complex workpieces meeting process requirements to meet the production needs of low-cost and small-batch production of large and complex products.
2. Due to the discretization of the forming head bodies, forming errors occur in the free deformation zone of the profile. The more die heads, the smaller the forming error. Under the same number of die heads, the forming error of the part arranged uniformly along the arc length is smaller than that arranged uniformly along the initial axial direction.
3. The fewer the number of dies, the easier the die adjustment. The minimum number of forming head bodies can be optimized for each bending radius to keep the forming error within the requirement range. The larger the bending radius of the profile, the fewer die heads are needed for forming.
4. Numerical simulation results match the experimental results well, and finite element numerical simulation can be used to predict forming accuracy and reduce production costs.

**Author contribution** Yu Wen: conceptualization, data curation; Ce Liang: investigation, writing—review and editing; Yi Li: data curation, investigation; Jicai Liang: methodology, data curation.

**Funding** This work was financially supported by Jilin Provincial Scientific and Technological Department (20220201048GX).

**Data availability** All information, figures, and tables are in the manuscript. It will not be necessary to provide other data and materials.

## Declarations

**Ethical approval** The author(s) declare that the article was constructed respecting all ethical conditions of publication.

**Consent to participate** All author(s) participated in the preparation of the article. In this way, the authors allow their names to be in the article.

**Consent for publication** The authors allow publication. All rights will belong to the journal.

**Conflict of interest** The authors declare no competing interests.

## References

1. Zhou W, Shao Z, Yu J, Lin J (2021) Advances and trends in forming curved extrusion profiles. Materials 14:1603. https://doi.org/10.3390/ma14071603
2. Rosenthal S, Maaß F, Kamaliev M et al (2020) Lightweight in automotive components by forming technology. Automot Innov 3:195–209. https://doi.org/10.1007/s42154-020-00103-3

3. Zhou W, Lin J, Dean TA, Wang L (2018) Feasibility studies of a novel extrusion process for curved profiles: experimentation and modelling. Int J Mach Tools Manuf 126:27–43. https://doi.org/10.1016/j.ijmachtools.2017.12.001
4. Vollertsen F, Sprenger A, Kraus J, Arnet H (1999) Extrusion, channel, and profile bending: a review. J Mater Process Technol 87:1–27. https://doi.org/10.1016/S0924-0136(98)00339-2
5. Welo T, Granly B (2010) A new adaptive bending method using closed loop feedback control. Trans Nonferrous Met Soc China 20:2111–2117. https://doi.org/10.1016/S1003-6326(09)60426-X
6. Chatti S, Hermes M, Tekkaya AE, Kleiner M (2010) The new TSS bending process: 3D bending of profiles with arbitrary cross-sections. CIRP Ann 59:315–318. https://doi.org/10.1016/j.cirp.2010.03.017
7. Hermes M, Chatti S, Weinrich A, Tekkaya AE (2008) Three-dimensional bending of profiles with stress superposition. Int J Mater Form 1:133–136. https://doi.org/10.1007/s12289-008-0009-0
8. Wu Jianjun Z, Zengkun S, Qi et al (2017) A method for investigating the springback behavior of 3D tubes. Int J Mech Sci 131–132:191–204. https://doi.org/10.1016/j.ijmecsci.2017.06.047
9. Welo T, Ma J, Blindheim J et al (2020) Flexible 3D stretch bending of aluminium alloy profiles: an experimental and numerical study. Procedia Manuf 50:37–44. https://doi.org/10.1016/j.promfg.2020.08.008
10. Ma J, Welo T (2021) Analytical springback assessment in flexible stretch bending of complex shapes. Int J Mach Tools Manuf 160:103653. https://doi.org/10.1016/j.ijmachtools.2020.103653
11. Zhang Q, Wang ZR, Dean TA (2008) The mechanics of multi-point sandwich forming. Int J Mach Tools Manuf 48:1495–1503. https://doi.org/10.1016/j.ijmachtools.2008.04.003
12. Li Y, Shi Z, Rong Q et al (2019) Effect of pin arrangement on formed shape with sparse multi-point flexible tool for creep age forming. Int J Mach Tools Manuf 140:48–61. https://doi.org/10.1016/j.ijmachtools.2019.03.001
13. Zhang Q, Dean TA, Wang ZR (2006) Numerical simulation of deformation in multi-point sandwich forming. Int J Mach Tools Manuf 46:699–707. https://doi.org/10.1016/j.ijmachtools.2005.07.034
14. Peng H, Li M, Liu C, Cao J (2013) Study of multi-point forming for polycarbonate sheet. Int J Adv Manuf Technol 67:2811–2817. https://doi.org/10.1007/s00170-012-4694-y
15. Liang J, Gao S, Teng F et al (2014) Flexible 3D stretch-bending technology for aluminum profile. Int J Adv Manuf Technol 71:1939–1947. https://doi.org/10.1007/s00170-013-5590-9
16. Liang J, Chen C, Li Y, Liang C (2020) Effect of roller dies on springback law of profile for flexible 3D multi-point stretch bending. Int J Adv Manuf Technol 108:3765–3777. https://doi.org/10.1007/s00170-020-05655-6